Transient states and the role of excited state self-quenching of indoline dyes in complete dye-sensitized solar cells

ARTICLE *in* DYES AND PIGMENTS · FEBRUARY 2015

Impact Factor: 3.97 · DOI: 10.1016/j.dyepig.2014.10.008

Dyes and Pigments 113 (2015) 692–701

Contents lists available at ScienceDirect

Dyes and Pigments

journal homepage: www.elsevier.com/locate/dyepig

Transient states and the role of excited state self-quenching of indoline dyes in complete dye-sensitized solar cells

Jan Sobuś [a, b], Jerzy Karolczak [b, c], Dariusz Komar [b], Juan A. Anta [d], Marcin Ziółek [b, *]

[a] NanoBioMedical Centre, Adam Mickiewicz University, Umultowska 85, 61-614 Poznan, Poland
[b] Quantum Electronics Laboratory, Faculty of Physics, Adam Mickiewicz University, Umultowska 85, 61-614 Poznan, Poland
[c] Center for Ultrafast Laser Spectroscopy, Adam Mickiewicz University, Umultowska 85, 61-614 Poznan, Poland
[d] Departamento de Sistemas Físicos, Químicos y Naturales, Area de QuímicaFísica, Universidad Pablo de Olavide, Ctra. Utrera, Km 1, E-41013 Sevilla, Spain

ARTICLE INFO

Article history:
Received 28 August 2014
Received in revised form
6 October 2014
Accepted 9 October 2014
Available online 18 October 2014

Keywords:
Indoline dyes
Dye sensitized solar cells
Ultrafast spectroscopy
Dye aggregation
Titanium dioxide nanoparticles
Zinc oxide nanoparticles

ABSTRACT

The photo behaviour of indoline dye D149 on different metal oxide nanoparticles in functioning solar cells is investigated by time-resolved studies in the time range from 100 fs to several ns. The cells are also characterized by standard photovoltaic measurements. The electron injection is found to occur on the time scales from <200 fs to several tens of ps. Locally excited (LE) and charge transfer (CT) excited states of the dye are identified to participate in the electron injection and dye deactivation mechanisms. The dependence of the ultrafast dynamics on the coadsorbent concentration and energy density of the pump pulse indicates the important role of excited state self-quenching. A decrease in the photocurrent of the cells upon aging (very fast for ZnO and slower for TiO_2 nanoparticles) is found to be correlated with the transient absorption kinetics, with a probable explanation suggested as electrolyte-induced dye rearrangement and aggregate formation.

1. Introduction

Indoline dye D149 [1] is a popular metal-free sensitizer used in dye-sensitized solar cells (DSSC) [2,3]. The best sunlight conversion efficiency of DSSC with this dye and iodine-based liquid electrolyte is 9% [4], which can be compared to record efficiencies of best metal-free dyes, 10.2% with iodine-based electrolyte [5], 10.65% with cobalt-based electrolyte [6], ruthenium dyes 11.7% [7], and porphyrin dyes, 13.0% [8]. Besides the high efficiency, D149 showed remarkable promising properties when used with less volatile ionic liquids, solid state electrolytes and alternative metal oxides [4,9–13]. DSSC systems with this dye were also widely studied in the context of the observed transient Stark shift [14–18]. Moreover, the new dyes containing indoline moiety have recently shown very high conversion efficiencies [6,19].

Dynamics and quantum yield of electron injection in DSSC, which can be studied by ultrafast laser spectroscopy techniques [20–28], are important parameters that might determine the sunlight conversion efficiency of the device [29,30]. This issue became even more important in recent years, when it was revealed that in many cases the rate of electron injection from the excited state of the dye to the conduction band of metal oxide is slower in the complete cells than in the isolated systems investigated before [31–35]. Therefore, since the characteristic time scale is often longer than sub-ps, many internal deactivation processes present in the dye might efficiently compete with electron injection and lower the photovoltaic performance of DSSC. In particular, we have recently shown that lower photocurrent of D149 solar cell with ZnO nanoparticles compared to those with TiO_2 ones is directly related to the ultrafast processes occurring in the first 500 ps and that electron injection is slower for ZnO cells than for TiO_2 [36].

D149 dye has been studied in solution by femtosecond transient absorption [37] and femtosecond up-conversion techniques [38]. These studies revealed a formation of charge transfer (CT) state in polar solvent and solvent-dependent decay of CT state. Moreover, picosecond fluorescence studies with time-correlated single photon counting(TCSPC) technique indicated the occurrence of isomerization process [39] and the excited-state proton transfer process [40] as responsible for the enhanced deactivation rate. Femtosecond up-conversion of D149 on TiO_2 films showed a decay of the first singlet excited state with the averaged time constant of about 2 ps [12]. A different conclusion was drown from femtosecond transient absorption studies of D149 (with the coadsorbent) on TiO_2 and ZnO films in the visible range [17]. In that studies the

* Corresponding author. Tel.: +48 61 829 5011.
E-mail address: marziol@amu.edu.pl (M. Ziółek).

http://dx.doi.org/10.1016/j.dyepig.2014.10.008
0143-7208/

ultrafast (<250 fs) dynamics of electron injection was observed, similar for both metal oxides. However, our recent investigation of complete solar cell of D149 without coadsorbent revealed much worse electron injection efficiency in ZnO than TiO_2 cells [36]. Next, for the reference system of D149 on ZrO_2 films fs transient absorption studies showed similar ultrafast (<250 fs) formation of a cation–electron complex (explained by the interaction of the dye with the trap states below ZrO_2conduction band) [17]. On the contrary, TCSPC studies of D149/ZrO_2 films showed excited state deactivation on the time scale of hundreds of ps (fast component) and single ns (slow component), with increasing lifetime for higher coadsorbent (chenodeoxycholic acid, CDCA) content [39]. The mid-infrared measurements in complete D149 solar cells indicated the double exponential <300 fs to 30 ps electron injection kinetics [34]. However, for high intensity of the pulses the kinetics became significantly faster [34].The above results, often in contradiction to each other, clearly show the need of further investigation of the dynamics of fully organic dyes, like D149, in DSSC to understand which processes play a key role in functioning devices.

Therefore, in this contribution we have significantly extended our previous study to better understand the ultrafast processes occurring in D149 molecule attached to metal oxide nanoparticles in complete solar cells. For comparison, we have also measured D149 in solution and on metal oxide films in air. The main novel features of the present studies are the following: (i) the femtosecond transient absorption measurements in the visible spectral range (450–800 nm) were performed with a higher signal-to-noise ratio and longer time window up to 3 ns; (ii) new femtosecond transient absorption studies in near-infrared (NIR, 800–1500 nm) spectral range were used; (iii) studies with different amount of coadsorbent and different pump pulse intensity were performed. All of these enabled us to better explain the differences between the dynamics in TiO_2 and ZnO solar cells, to understand the discrepancy between previous ultrafast results of D149, and to discover new processes and transient states in D149 relevant for efficient electron injection. We believe that our studies enable better understanding the photophysics of indoline dyes interacting with inorganic nanomaterials. Moreover, the mechanisms we found should be relevant for many all-organic dyes with high extinction coefficient used in DSSC and our findings are important for improving solar cell efficiency in general.

2. Materials and methods

Indoline dye D149, chenodeoxycholic acid (CDCA) and Al_2O_3 nanoparticles (diameter <50 nm) were purchased from Sigma–Aldrich. ZnO (VP ZnO20) and TiO_2 (P25) nanoparticles were received from Evonik. The procedure of preparing the paste with oxide nanoparticles was the same for all the materials, with the exception of acetic acid content: it was 0 ml for ZnO, 0.5 ml for TiO_2 and 1 ml for Al_2O_3. Pastes were prepared as follows. First 3 g of nanoparticles powder was mixed with acetic acid, 20 ml of ethanol and left in ultrasonic bath for 3 h. Then another solution of 10 ml α-terpineol, 1.5 g of ethyl cellulose and 13.5 g of ethanol was prepared. Two solutions were mixed together and placed in ultrasonic bath for another hour. Afterwards they were stirred for 16 additional hours. Finally, the ethanol was removed with a rotary evaporator operating at 60 °C and the ready to use paste was obtained.

The films were deposited by doctor-blade technique on fluorine doped tin oxide (FTO) glass plates and heated at 450 °C (TiO_2 and Al_2O_3) or 420 °C (ZnO) for 60 min. Then, the films were immersed in a 0.2 mM solution of D149 with different concentrations of CDCA (0 mM, 0.2 mM and 2 mM) in acetonitrile (ACN): tert-butanol mixture (1:1) and kept at room temperature for about 1 h. The platinised counter electrode was obtained by spreading a Pt-based solution (Platisol T, Solaronix SA) on FTO glass and annealing at 450 °C. The transmission of Pt layered electrode varies from 75% at 450 nm to 90% at 800 nm with respect to pure FTO glass. To make a complete solar cell (the active area of 1.1 cm^2 was prepared), the counter electrode was assembled with thermal adhesive film (25 μm Surlyn, Meltronix, Solaronix SA) that acts as separator and sealing element. The cells were filled (by vacuum backfilling method) with a commercial liquid electrolyte (Iodolyte AN-50, Solaronix SA) containing the I^-/I_3^- redox couple ($[I_2] = 50$ mM) in ACN solution.

For ultrafast transient absorption experiments a commercial femtosecond broadband transient absorption spectrometer (Helios, Ultrafast Systems) was used in a single-beam configuration, with all reflective white light continuum generator and depolarizer in the pump beam to avoid influence of rotational dynamics. The femtosecond pulses were provided by Spectra Physics setup consisting of MaiTai SP oscillator, Spitfire Ace amplifier (pumped by Empower laser) and Topas Prime wavelength convertor (optical parametric amplifier). The pump pulses were at 555 nm and the IRF (pump-probe cross correlation function) was 250–300 fs (FWHM). The typical pump pulse energy was 500 nJ, corresponding to energy density of about 1 mJ/cm^2. In some experiments 200 nJ and 2 μJ pulses were also used. The probe light continuum was generated in sapphire or YAG-type crystal. All the spectra analyzed were corrected for chirp of white light continuum. The transient absorption measurements were performed in the spectral ranges 450–800 nm (VIS) and 800–1500 (NIR) and in the time range of up to 3 ns.

The transient absorption spectra are the combination of positive signals originating from the absorption of transient species, negative signals due to ground state depopulation (corresponding spectrally to steady-state absorption bands), and negative signals due to stimulated emission from the excited state (occurring for the wavelength for which steady-state emission is present). To analyze the transient absorption dynamics in more detail, we used a global approach. The global analysis of the data was done using Surface Explorer program (Ultrafast Systems) which fits multi-exponential function (convoluted with IRF of our setup, FWHM between 250 and 300 fs) to the kinetic vectors of selected number of singular values and reproduces the spectra of the amplitudes associated with the time components. As a result, the characteristic time constants are revealed for the whole spectral range investigated (in our case combined VIS and NIR regions), and the wavelength-dependent amplitudes associated with these time constants are obtained (also called decay associated difference spectra). The positive value of the amplitude at certain wavelength indicates a change towards less positive (or more negative) transient absorption signals at this wavelength, while a negative value of amplitude indicates opposite. In all figures presenting transient absorption spectra the time zero (maximum of IRF) is set at 0 ps, while for all figures showing kinetic traces it is shifted to 1 psin order to present the time axis in logarithmic scale.

Analysis at particular probe wavelength was done by fitting stretched exponential function (convoluted with IRF) to the transient absorption signals. The function is defined as:

$$A\left(t\right) = A_0\, e^{-(t/\tau)^{\beta}}. \tag{1}$$

This function contains two parameters: the characteristic time τ and the dispersion parameter β ($0<\beta<1$, lower β values mean more stretched decay, extending the decay time scale). The average time of the process described by function (1) was calculated as:

$$\tau_{AVG} = \frac{\tau}{\beta}\Gamma\left(\frac{1}{\beta}\right). \tag{2}$$

We should note that sometimes the averaged time constant from stretched exponential fit given by Eq. (2) is not a good parameter to compare when the dispersion parameter differs too much (for example, for one sample $\beta > 0.7$ and another $\beta < 0.4$, in the latter case the averaged lifetime is too long). Therefore, in all tables in which the decay parameters are shown, a half-decay time is also given.

The time-resolved emission measurements in the picosecond time window were performed using a time correlated single photon counting technique (TCSPC) [41]. The measurements were carried out at the magic angle with the pump wavelength of 425 nm. The analysis was done by fitting stretched exponential function (Eqs. (1)–(2)) convoluted with the IRF of the setup (measured by light scattering of the same samples at pump wavelength) to the fluorescence decays at the wavelength around 660 nm (corresponding to the maximum of emission band). The steady-state UV–visible absorption spectra were measured with a UV-VIS-550 (Jasco) spectrophotometer. An M101 potentiostat with FRA32M module (Autolab) was used to measure electrochemical impedance spectra (10 mV perturbation in the 10^{-1}–10^{6} Hz range) in the dark and at open circuit, and the data sets were analyzed with Nova 1.10 (Autolab) software. The potentiostat was also used to measure current–voltage (J–V) curves under the irradiation of white light LED lamp. The distance between the LED lamp source and the solar cell was adjusted to give a photocurrent corresponding to that obtained in the control experiment for the same samples at 1 Sun conditions using a solar simulator (Sun 2000 class A, Abet Technologies, equipped with an AM 1.5 G filter). The morphology of the nanoparticle films was analyzed using a Scanning Electron Microscope (JEOL 7001 TTLS).

3. Results and discussion

3.1. Photovoltaic performance, steady-state spectroscopy and time-resolved emission studies

Table 1 collects the most important parameters of the cells prepared with TiO_2, ZnO and reference Al_2O_3 films (all sensitized with 0.2 mM D149 and 2 mM CDCA). The trend is similar to that reported by us previously for the D149 cells prepared without coadsorbent and with different TiO_2 and ZnO pastes [36]. The relatively low short circuit current of D149/TiO_2 cell ($J_{sc} = 4$ mA/cm^2 under conditions similar to those of AM1.5 (1 Sun) is mainly due to limited absorbance of the sensitized metal oxide layer (absorbance of about 1 at the maximum of D149 band) required in our time-resolved studies. D149/TiO_2 cells prepared without CDCA showed about 50% higher absorption and 20% higher J_{SC}.

Table 1
Photovoltaic parameters of the samples using 2 mM CDCA: amplitude (A_{max}) and wavelength (λ_{max}) corresponding to the maximum of the D149 absorption band, thickness of the mesoporous layer (d), open circuit voltage (V_{OC}), short circuit current density (J_{SC}) for 1 Sun conditions, fill factor (FF), number of absorbed photons (N_{ph}) calculated as previously [36], and J_{SC}/N_{ph} ratio.

Sample:	TiO_2	ZnO	Al_2O_3
A_{max}	1.0	0.3	1.2
λ_{max}, nm[a]	516	505	507
d, μm	3	1	3.5
V_{OC}, mV	630	600	200
J_{SC}, mA/cm^2	4.0	0.80 → 0.15[b]	0.05
FF	0.45[c]	0.60	–
N_{ph}, x10^{16}, s^{-1}cm^{-2}	6.06	3.18	6.86
J_{SC}/N_{ph}, x 10^{-16}, mA/s	0.66	0.25 → 0.05[b]	0.01

[a] Films in air.
[b] Decrease after 1 day.
[c] $FF = 0.55$ after series resistance correction.

The absorbance of the dye in ZnO cells is smaller than that of TiO_2. The initial photocurrent per number of absorbed photons (J_{sc}/N_p in Table 1) of D149/ZnO cells is 2–3 times lower than that of D149/TiO_2 cells. However, the photocurrent drops rapidly. 2 h after preparation it is only 30–40% of its initial value, and after 1 day it is only 20%. On the contrary, for D149/TiO_2 cells we observed a drop of the photocurrent of the same magnitude that in D149/ZnO after 2 weeks instead of 2 h. Due to the measurements duration, all time-resolved studies of complete D149/ZnO cells presented in next sections correspond to the conditions at which the relative photocurrent (per absorbed photons) is about 10 times smaller than that of TiO_2 samples. We have checked that D149 dye molecules can be dissolved from ZnO film as indicated before [42]. As shown in Fig. S1A (in the supporting information, SI), the absorption of D149/ZnO film decreases by about 40% after 20 h immersion in neat acetonitrile (similar for the films sensitized with and without CDCA addition). This might be the reason for quick lowering of the photocurrent in D149/ZnO cells. However, as will be revealed in next sections, the explanation is probably more complex.

Finally, the reference D149/Al_2O_3 cells show some small, but nonzero photocurrent (Table 1, about 1% to that of D149/TiO_2 cells), in similar fashion as found by us previously [36]. The origin of this photocurrent might be either due to the presence of very deep trap states below conduction band in alumina or due to the presence of trace impurities in commercial Al_2O_3 nanopowder. We have checked that the Al_2O_3 cells without D149 dye give no photocurrent at all, so it is certainly due to the electrons transferred from the excited dyes.

Exemplary SEM pictures of the surface of metal oxide layers and their cross-sections are presented in Fig. S2. They show that the thickness of the TiO_2 layer (3 μm) is about 3 times larger than that of ZnO (1 μm). We also used electrochemical impedance spectroscopy to characterize the cells and metal oxide layers. The results are shown in supporting information (Table S1 and Fig. S3–S5). The charge recombination in ZnO layer is slightly slower than that of TiO_2 for the corresponding bias voltages, but for both materials the relative diffusion length (the ratio of the diffusion length over the nanoparticle layer thickness) is always larger than 3, indicating good collection efficiency.

The effect of adding coadsorbent to the sensitizing solution on the steady-state absorption spectra is shown in Fig. 1A and Fig. S1B. The absorption band of D149 is shifted slightly to the blue when more CDCA is added, in accordance to the previous report [43]. For D149/TiO_2 film the maximum changes from 523 nm (no CDCA) to 516 nm (2 mM CDCA), while for D149/Al_2O_3 the corresponding change is from 521 nm to 507 nm. The small absorption changes lie in contrast with our recent studies of NIR absorbing dye HY103 [44]. In that case, even upon small addition of CDCA (0.2 mM), a drastic change in steady-state absorption spectra was observed due to the diminish of H-aggregates band (on the short-wavelength side of monomer's band). However, as will be shown in next sections, the impact of CDCA addition on the transient kinetics of D149 is much higher than it could be expected from the steady-state spectra.

We performed TCSPC experiments to check the effect of coadsorbent for D149/TiO_2 cells (Fig. 1B). As can be seen, upon the addition of CDCA the fluorescence decay becomes longer with the average decay times equal to 50 ps for the samples without CDCA, 90 ps for 0.2 mM CDCA and 170 ps for 2 mM CDCA. It indicates the possible competing quenching process which will be further explored in next sections. We also compared the fluorescence decays for cells with different metal oxides for moderate CDCA concentration (0.2 mM CDCA, Fig. S6). The trend is similar to that reported by us previously for the cells without CDCA [36]. The

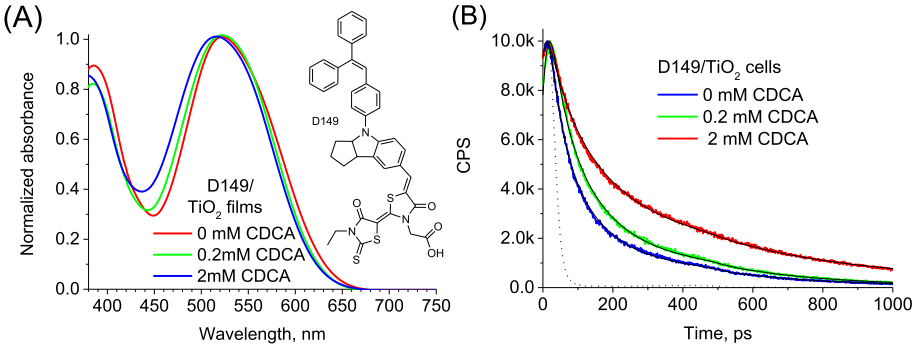

Fig. 1. (A) Steady-state absorption spectra of D149/TiO_2 films for different concentrations of coadsorbent (CDCA) in the sensitizing solution. The inset shows the structure of D149 molecule. (B) Fluorescence decays obtained in TCSPC experiment at 660 nm after 425 nm excitation for D149/TiO_2 cells with different concentration of coadsorbent. The black line shows the best fit using stretched exponential function with parameters given in Table S2A.

averaged decay time is 200 ps for D149/Al_2O_3, 170 ps for D149/ZnO and 90 ps for D149/TiO_2 cells. The electron injection yield calculated on the basis of such values is equal to 55% for D149/TiO_2 cells and much smaller (15%) for D149/ZnO cells.

3.2. Transient absorption studies

3.2.1. D149 in solution and D149/Al_2O_3 cells

Transient absorption studies of D149 in solution are presented in the supporting information (text and Fig. S7). The spectra of all fitted components in global analysis are presented in Fig. 2A. The most important information for further studies of DSSC are the following. Two excited states of D149 with different spectral characteristics are identified. The decay of the first one, LE state, with time constant 0.4 ps is accompanied by the positive amplitudes with maximum around 720 nm in the VIS range and positive amplitudes for wavelength <1100 nm and >1450 nm in NIR range. The decay of subsequent and relaxed CT state is connected with the positive amplitudes with maxima around 600 nm and 1370 nm, and is clearly mono-exponential (time constant 420 ps). The absorption from both states has a significant contribution in the NIR range (in fact their extinction coefficients in NIR are comparable to those in VIS range). In studies of some DSSC it is assumed that only radical cations and electrons in metal oxide conduction band give contributions to the signals in NIR and, thus, the rise of such signals can be directly related to the electron injection dynamics. Our transient absorption results in NIR clearly show that it is not in the case of D149 dye, and probably in the whole family of indoline dyes, because the strong transient absorption signals from the excited states are also present in this range.

For D149/Al_2O_3 reference cells (with 0.2 mM CDCA) we do not expect significant contribution of electron injection, although the nonzero photocurrent mentioned above indicates the possible small contribution of a charge separation process. The global analysis (Fig. 2B) brings three time components of $\tau_1 = 0.2$ ps, $\tau_2 = 3.0$ ps and $\tau_3 = 65$ ps as well as the fourth component ($\tau_4 > 1$ ns) which represents the residual signal, constant in the time window of our setup. Interestingly, the complex wavelength-dependent spectra indicate that the decay of the dye attached to alumina cannot be simply explained by the decay of one excited state, even if the vibrational relaxation and cooling are taken into account. On the contrary, the amplitude spectra of all three components are positive in the region above 600 nm, up to 1500 nm, and we can observe two distinguished spectral features which relative contribution changes for different time constants. For short time constants ($\tau_1 = 0.2$ ps and $\tau_2 = 3.0$ ps) a dominant feature is one with a maximum around 720 nm, while for the longer component ($\tau_3 = 65$ ps) the main band is that with a maximum around 600 nm. The spectral similarity in VIS region to those observed in solution (and discussed above) suggests that we also observe LE and CT states for D149/Al_2O_3 cells. It should be noted that the decays of LE and subsequent CT states are not mono-exponential and they both contribute to the amplitude spectra of more than one component from the global fit. In particular, the band at 720 nm (LE) is present not only in τ_1 spectra, but also in those of τ_2 and τ_3 components (but with decreasing contribution). Similarly, the CT band at 600 nm is observed not only in τ_3 spectra, but also in shorter τ_2 spectra.

A decay of LE in NIR is manifested as positive amplitudes of $\tau_1 = 0.2$ ps component for wavelengths<1100 nm and >1300 nm, similar to those of D149 in solution. As for CT state, which is abundant in amplitude spectra of longer components (τ_2 and τ_3), its band in NIR is significantly spectrally broader than that observed in solution. The possible explanation is that the nature of CT state is slightly different when the molecules are chemically bonded to semiconductor surface. Probably, the LUMO orbital extends more towards the metal oxide structure (in this case Al atoms) and the absorption spectra in NIR are especially sensitive to such changes [45]. The CT state might be therefore more like exciplex nature, rather than bound radical cation–electron complex, maintaining its electronically excited state character with respect to the dye. The residual component (τ_4) with positive maxima at around 630 nm and 1100 nm (and negative ground state depopulation maximizing at around 500 nm, Fig. 2B) clearly shows that some portion of the excited dyes do not relax to the ground state but, most probably, inject electrons to deep trap states in alumina, possibly due to the presence of impurities or surface defects. Therefore, we might assign the residual spectra to the bounded complex between dye and trapped electrons. Eventually, in some portion of these complexes, further charge separation might occur giving rise to the small photocurrent observed in D149/Al_2O_3 cells (as found in the previous section).

3.2.2. D149/TiO_2 and D149/ZnO cells

For D149/TiO_2 cells with 0.2 mM CDCA (Fig. 2A and S8A-B) the time constants of globally fitted components ($\tau_1 = 0.2$ ps, $\tau_2 = 3.5$ ps, $\tau_3 = 70$ ps and $\tau_4 > 1$ns) do not differ too much from those obtained for D149/Al_2O_3 cells, which is consistent with our previous report for the cells without CDCA [36]. However, more detailed investigation shows that it is rather the coincidence due to spreading of the dynamics over many time scales in both systems, while the main difference lies in the relative amplitudes between the components of both cells. Indeed, the final, residual signal (amplitude of τ_4 component) is much higher than that found in

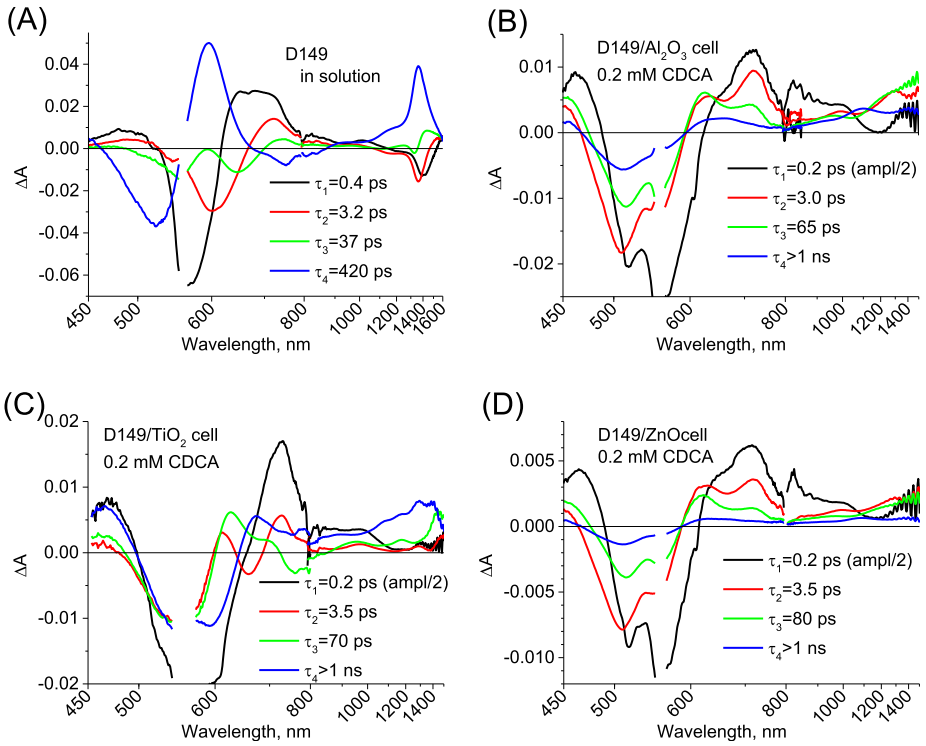

Fig. 2. The wavelength-dependent amplitudes of the components with time constants given in the inset obtained by multi-exponential global fit for (A) D149 in ACN:tert-butanol (1:1) solution (B) D149/Al_2O_3, (C) D149/TiO_2, and (D) D149/ZnO cells. In (B)–(D) cases the concentration of CDCA was 0.2 mM and the amplitude of the fastest component ($\tau_1 = 0.2$ ps) is decreased by 2 because the fitting procedure makes it larger due to the convolution with comparable IRF (FWHM = 0.25–0.3 ps).

D149/Al_2O_3 cells (see also Fig. 2B). Moreover, the spectrum of this component is also different: the negative signal extends further into long-wavelength range (up to 630 nm, while for D149/Al_2O_3 it was up to 580 nm), the maximum in the visible range is shifted to 670 nm, and the signal in NIR contains dominant features for wavelengths around 1300 nm. All of these differences can be explained by the fact that for D149/TiO_2 cells with efficient electron injection a large concentration of D149 radical cation is present, the electrons in titania conduction band contribute to the signal (especially in NIR range), and there is a transient Stark shift signal originating from the electric field created by the electrons in the semiconductor. The latter is responsible for the transient features having the shape of first derivative of steady-state absorption band, which results in the apparent shift of the negative transient absorption band towards the red [18]. The differences in the VIS range are similar to those previously reported in transient absorption studies of D149 in films [17]. In these studies the transient Stark shift was observed for D149/TiO_2 and D149/ZnO samples, while it was absent for D149/ZrO_2 samples.

The efficient creation of D149 radical cation is also revealed in the shape of the amplitudes of $\tau_2 = 3.5$ ps and $\tau_3 = 70$ ps components. Unlike their analogues in D149/Al_2O_3 cells, they contain negative regions for $\lambda > 600$ nm, which indicate a rise of the signal due to higher extinction coefficient of the D149 radical cation than that of CT state for these wavelengths. For the $\tau_2 = 3.5$ ps component a rise occurs in the range 630–680 nm, while for $\tau_3 = 70$ ps a rise is present in the range 720–850 nm. In the latter case the rise might be also due to the changes in the radical cation spectrum due to the hole transfer within its structure [46].

Besides the clear formation of radical cation from CT state, our present data also indicates partial, faster electron injection from LE state. This state decays much faster in D149/TiO_2 cell than in the reference D149/Al_2O_3 cell. Although the time components from global analysis are similar, the feature at 730 nm (characteristic for LE state) contributes mainly to the spectra of$\tau_1 = 0.2$ ps and, a little bit, to $\tau_2 = 3.5$ ps components for D149/TiO_2 sample (Fig. 2C), while for D149/Al_2O_3 sample the contribution is comparable for $\tau_1 = 0.2$ ps and $\tau_2 = 3.0$ ps spectra, and it is also present in $\tau_3 = 65$ ps spectra (Fig. 2B). This difference can also be directly visualized when the transient kinetics at 730 nm are compared. This is presented in Fig. 3A together with the stretched exponential fit, whose results are shown in Table 2A. The average decay time is about 10 times faster for D149/TiO_2 samples (0.7 ps) than for D149/Al_2O_3 ones (8.0 ps).

Next, we present the global fit results of D149/ZnO cells with 0.2 mM CDCA (Fig. 2D and S8C-D). Also in line with our previous report [36], the spectra and time constants are similar to those found for reference D149/Al_2O_3 cells, consistent with the poor photocurrent in D149/ZnO cells. The decay of LE state in D149/ZnO cell is only slightly faster than that in D149/Al_2O_3 and much longer than for D149/TiO_2 cells (kinetics at 730 nm, Fig. 3A), indicating a significantly slower injection for ZnO cells. There is no indication of transient Stark signal, and the residual signal in both VIS and NIR ranges is very small ($\tau_4 > 1$ ns component), with the spectral shape more similar to that of D149/Al_2O_3 (possible bounded complex between dye and trapped electrons) than D149/TiO_2 cells (separated radical cations and electrons in conduction band).

One of the explanations for poor performance of D149/ZnO cells might be the before-mentioned detachment of dyes from ZnO surface in the presence of solvent. However, we do not observe any indication of free dyes in electrolyte, whose presence should appear as mono-exponential long decay. On the contrary, the decay of transient absorption signal in D149/ZnO cells for wavelengths corresponding to the CT state is even faster than in two other cells with high dispersion parameter (see, for example, kinetics at 630 nm presented in Fig. 3B), pointing out the enhanced excited

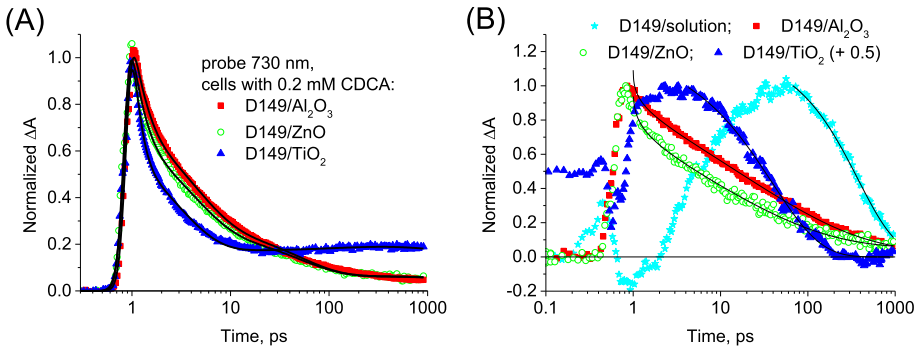

Fig. 3. Kinetic traces of transient absorption measured for the indicated samples (D149 in solution and different cells with 0.2 mM CDCA) at (A) 730 nm and (B) 630 nm. The pump pulse was 0.5 μJ at 555 nm. The black line shows best fit with parameters given in Table 2. In (B) the fit was without convolution with IRF and the kinetics for D149/TiO_2 were shifted upwards by 0.5 to better show the differences in the time scale of the decay. The time zero is shifted to 1 ps in order to present the time axis in logarithmic scale.

state self-quenching in D149/ZnO cells. We will come back to these interesting features below.

3.2.3. *Light intensity and coadsorbent concentration dependence*

Now we will present the effect of different excitation pulse energy and CDCA concentration for the complete cells. Fig. 4A presents transient absorption kinetics probed at 1300 nm with different intensities of pump pulse for D149/TiO_2 cells without CDCA. As shown before, both excited LE and CT states of D149 probably contribute to the transient absorption signal at this wavelength. The parameters of the fitted decay are collected in Table 3. As can be seen, a strong dependence on excitation intensity is observed for both the decay time and the residual signal (3 ns after excitation). The latter signal corresponds to the combined absorption of D149 radical cations and electrons in the semiconductor, so its relative amplitude (with respect to the initial signal) is proportional to the efficiency of electron injection (assuming that the initial signal does not contain significant contribution from electron injection products, which means that electron injection from LE state in times below 100 fs can be neglected). Increasing the energy of the pump pulse 10 times (from 0.2 μJ to 2 μJ, corresponding to the change in excitation fluence from 0.4 mJ/cm^2 to 4 mJ/cm^2) results in about a 10-fold decrease in characteristic time of stretched exponential decay and decrease of its dispersion parameter (from 0.6 to 0.3, making the decay more stretched). Moreover, the electron injection efficiency drops 2 times (residual signal decreases from 52% to 27%). The most likely explanation is that a significant contribution of excited state self-quenching occurs, with singlet–singlet annihilation mechanism being the most probably explanation. Indeed, this process, competing with electron injection, was proposed to be responsible for deactivation of dyes in DSSC systems before [47–49]. Since it is a second order process with respect to the concentration of excited species, its rate is proportional to the excitation intensity, which is being observed by us in the current studies (Fig. S9B). To confirm this hypothesis we repeated the same experiments for reference D149/Al_2O_3 cells without CDCA. Indeed, the results presented in Fig. 4B and Table 3B indicate a similar behavior in a system where dye molecules are densely packed on nanoparticles and there is no significant injection (as mentioned above).

Table 2
Values of the parameters of the best stretched exponential function given by Eqs. (1)–(2) fitted to the transient absorption signals of different cells with 0.2 mM CDCA. The pump pulse energy was 0.5 μJ and probe wavelength was 730 nm (A) and 630 nm (B). Last column presents half-decays of the kinetics.

Sample:	τ/ps	β	τ_{AVG}/ps	$\tau_{1/2}$/ps
(A)				
D149/TiO_2 cell	0.32	0.47	0.72	0.4
D149/ZnO cell	0.83	0.32	5.8	1.5
D149/Al_2O_3 cell	1.29	0.33	8.0	2.2
(B)				
D149/ACN + t-but solution	400	1.00	400	300
D149/TiO_2 cell	40	0.78	46	30
D149/ZnO cell	10	0.33	62	5
D149/Al_2O_3 cell	25	0.34	139	17

Furthermore, the rate of excited state self-quenching of dye molecules is the rate of the energy transfer from one singlet to another singlet state, so it should depend on the average distance between the molecules too. This is exactly confirmed in our experiments with D149/TiO_2 cells with different CDCA concentration. Representative kinetics at 1300 nm are presented in Fig. 5A together with the fitted function of parameters collected in Table 4A. The trend with increasing CDCA concentration (thus increasing the averaged distance between D149 dyes) is the same as that of decreasing pump pulse intensity: longer decay and higher electron injection yield. For the reference D149/Al_2O_3 cells with 2 mM CDCA the transient absorption measurements with different excitation energies were also made (Fig. S9A and Table S3). The decay is longer than that for the samples without CDCA for the corresponding energies (compare Figs. S9A and 5B). The dependence on the energy is smaller, but it is still present, which means that even for relatively high CDCA concentration the self-quenching is still present to some extent. The interaction of closely packed D149 molecules forming some type of aggregates is probably reflected in steady-state absorption spectra as slight red-shift of absorption band with smaller CDCA concentration (Fig. 1A and S1B).

On the contrary, the transient absorption kinetics for D149/ZnO cells exhibit a small dependence on the CDCA concentration (Fig. 5B and Table 4B). The residual signal is small (about 5% of that of the initial amplitude at 1300 nm) in line with the poor photocurrent of the ZnO cells. The characteristic decay time constants are shorter and the dispersion parameters are smaller than those for D149/TiO_2 and D149/Al_2O_3 cells. This is in line with faster quenching shown in Fig. 3B (kinetics at 630 nm) as discussed in the previous section. Again, we do not observe any contribution of the free dyes in solution (that have longer lifetimes). Our explanation is that D149 molecules are easily detached from ZnO surface in the presence of liquid electrolyte in complete cells (see also Fig. S1A). However, they do not stay free in the electrolyte but they attach again to the places close to other D149 molecules forming a type of aggregations, probably enhanced by ionic shells around other dyes. In such conditions they suffer from huge self-quenching and do not inject electrons efficiently. Therefore, irrespectively of the initial

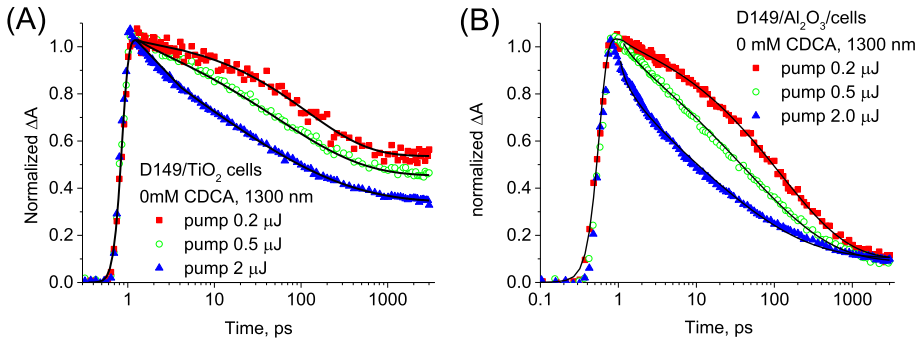

Fig. 4. Kinetic traces of transient absorption measured at 1300 nm for (A) D149/TiO_2 and (B) D149/Al_2O_3 cells at the indicated pump pulse energies (at 555 nm). The cells were without coadsorbent. The black line shows best fit with parameters given in Table 3. The time zero is shifted to 1 ps in order to present the time axis in logarithmic scale.

distribution of D149 molecules and coadsorbent presence, after immersion in electrolyte a new distribution is being formed, and quickly appearing D149 aggregates are responsible for the fast drop of photocurrent in D149/ZnO cells. We think that this is a second reason for the bad performance of DSSC made of ZnO semiconductor and D149 dye, apart from the slower electron injection reported by us before [36].

Finally, we measured NIR transient absorption for old D149/TiO_2 cells (with 2 mM CDCA). Two weeks after preparation J_{SC} of such cells drop from 4.0 mA/cm^2 to 1.7 mA/cm^2. As can be seen in Fig. 5A and Table 4, the residual signal at 1300 nm is about 3.5 times smaller (in accordance with the decrease of the photocurrent) and the decay is faster than that of the fresh sample. It is also supported by the global analysis in NIR range shown in Fig. S10: for the fresh cell the fastest time component ($\tau_1 = 0.6$ ps) has positive amplitudes for $\lambda < 1100$ nm and $\lambda > 1400$ nm while for the old cell the amplitudes are also positive between 1100 and 1400 nm (indicating self-quenching of LE and/or CT state). Similarly, the contribution of the decay of the second fastest component ($\tau_2 = 14$ ps) is larger for older sample than for the fresh one. So, most probably, the decreased photovoltaic performance of aging D149/TiO_2 cells is connected with the same mechanism as for ZnO cells: electrolyte assisted formation of dye aggregates and enhanced excited state self-quenching. However, in the case of TiO_2 such process occurs much slower than for ZnO (weeks instead of hours), due to the stronger chemical interaction of the D149 dye with TiO_2 surface.

3.2.4. D149 in films

In this section, we would like to present control transient absorption experiments conducted on fresh TiO_2, ZnO and Al_2O_3 films sensitized with D149 dye. All samples were studied in air within 1 h after preparation, so the effect of water absorption was minimized.

Table 3
Values of the parameters of the best stretched exponential function given by Eqs. (1)–(2) fitted to the transient absorption signals of (A) D149/TiO_2 cells and (B) D149/Al_2O_3 cells (both without CDCA and for varying pump pulse energies). The probe wavelength was at 1300 nm. Last two columns present half-decays of the kinetics and ratio of residual signal amplitude to the initial amplitude.

Pump energy/μJ	τ/ps	β	τ_{AVG}/ps	$\tau_{1/2}$/ps	Residual signal/%
(A)					
0.2	121	0.61	179	59	52
0.5	56	0.43	152	44	41
2	14	0.29	140	11	27
(B)					
0.2	124	0.51	243	68	9.5
0.5	45	0.39	156	22	8.0
2	11.6	0.32	83	5	9.3

The global analysis results in combined VIS-NIR range for D149/TiO_2 film (0.2 mM CDCA) are presented in Fig. 6A. The differences from the complete D149/TiO_2 solar cell (analogous spectra in Fig. 2C) are probably due to significantly faster electron injection in films (see the discussion in the supporting information).

A very interesting feature can be observed in NIR transient absorption of D149 on different metal oxides (samples with 2 mM of CDCA). The representative kinetics shown in Fig. 6B (for the probing wavelength 1300 nm) indicates that the amplitude of residual signal is very similar for D149/TiO_2 and D149/ZnO films, and much higher than that of D149/Al_2O_3 films. Moreover, the global analysis in NIR range (Fig. S11B-D) for these samples confirms the similarity of the spectra of residual component for TiO_2 and ZnO films, both in the relative amplitude and in the shape (with the increasing contribution of free electrons in the conduction band with increasing wavelength). It is unlike the results in complete cells for which the spectra of D149/ZnO cells with poor photocurrent were rather similar to those of reference D149/Al_2O_3 cells. This interesting feature further supports our explanation that the fast decrease in J_{SC} in D149/ZnO cells is due to the detachment of dyes and the formation of aggregates under the presence of electrolyte. Indeed, in ZnO films (where electrolyte is not present) the electron injection yield is much higher.

3.2.5. Relation to DSSC working conditions

There is a huge difference in the excitation intensity in the time-resolved setups used in our experiments: the pump pulse fluence is only about 30 μJ/cm^2 in TCSPC, while it is about 1 mJ/cm^2 in transient absorption, greatly enhancing singlet–singlet annihilation process in the latter case. This might explain why in the transient absorption experiments the CT state of D149/ZnO cells decays faster than that of D149/TiO_2 (e.g. Figs. 3B and 5) while in TCSPC experiment it is the opposite (Fig. S6). Faster decay of D149 excited state under higher pump pulse intensity implies similarly faster apparent electron injection. This might be the reason why the rise of absorption conduction band electrons probed in mid-IR range (studies in complete cells but on sapphire substrate) was observed to be faster for sufficiently high excitation fluence [34]. Moreover, the excited self-quenching process might also explain the differences between previous results of D149 obtained by TCSPC and pump-probe techniques described in the introduction.

It is always an important question how the conditions in laser spectroscopy studies with pulsed excitation correlate with those under continuous sunlight irradiation. In our transient absorption experiment the excitation with 0.5 μJ pump (1 mJ/cm^2) corresponds to the injection of about 20 electrons per nanoparticle. It is similar to the typical value of 10 electrons per nanoparticle under normal working conditions of DSSC [3]. So, from the point of view

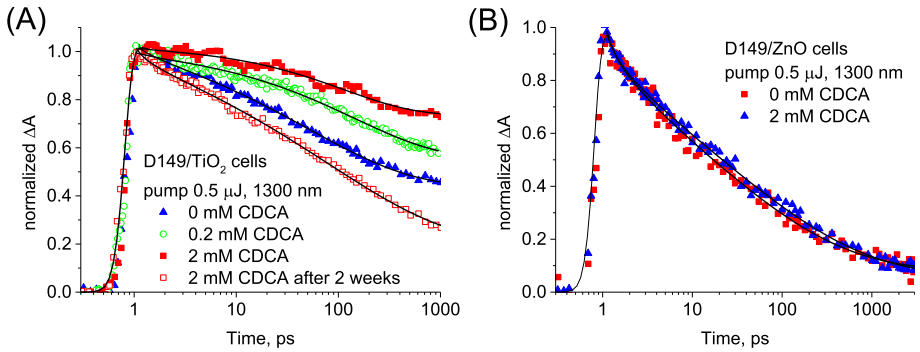

Fig. 5. Kinetic traces of transient absorption measured at 1300 nm for (A) D149/TiO_2 and (B) D149/ZnO cells with the indicated concentration of coadsorbent. The pump pulse was 0.5 μJ at 555 nm. The black line shows best fit with parameters given in Table 4. The time zero is shifted to 1 ps in order to present the time axis in logarithmic scale.

Table 4
Values of the parameters of the best stretched exponential function given by Eqs. (1)–(2) fitted to the transient absorption signals of (A) D149/TiO_2 cells, (B) D149/ZnO cells (both for different CDCA content) and (C) D149 films on different metal oxides (with 2 mM CDCA). The pump pulse energy was 0.5 μJ and probe wavelength was at 1300 nm. Last two columns presents half-decays of the kinetics and ratio of residual signal amplitude to the initial amplitude.

Cell:	τ/ps	β	τ_{AVG}/ps	$\tau_{1/2}$/ps	Residual signal/%
(A)					
no CDCA	56	0.43	152	58	41
0.2 mM CDCA	147	0.53	270	66	56
2 mM CDCA	117	0.63	164	72	72
2 mM CDCA[a]	87	0.37	370	46	19
(B)					
no CDCA	14	0.27	200	8	7
2 mM CDCA	21	0.27	350	11	5
(C)					
D149/TiO_2 film	26.5	0.41	82	12	34
D149/ZnO film	9.4	0.29	102	5.5	30
D149/Al_2O_3 film	85	0.37	355	38	3

[a] After 2 weeks, J_{SC} decreased from 4.0 to 1.7 mA/cm^2.

of number of electrons per particle, the photo behaviour observed in transient absorption is probably more relevant than that found in TCSPC experiments. However, under photostationary conditions the concentration of the transient species is proportional to its lifetime [50], so the concentration of excited dyes per particle is several orders of magnitude smaller than concentration of electrons. Therefore, from the point of view of excited state self-quenching, the conditions of TCSPC experiments are more relevant to 1 Sun.

Assuming average 20 nm diameter of TiO_2 nanoparticles and 50% porosity of the layer, the calculated dye coverage of D149/TiO_2 cells with 2 mM CDCA is 8×10^{13} cm^{-2}, which corresponds to the average distance between the dyes equal to 1.1 nm. When 20 photons are absorbed per nanoparticle in transient absorption experiment (with 0.5 μJ), the average distance between the excited molecules is 4.0 nm, which lies in the limit of efficient resonant energy transfer (<10 nm).

On the other hand, we would like to stress out a direct correlation between the relative amplitude of the residual transient absorption signal (high for fresh D149/TiO_2 cells and low for D149/ZnO and old D149/TiO_2 cells) and the photocurrent measured in exactly the same solar cells. This indicates that this process is still responsible for the real performance of solar cell made with indoline dyes, although the rates of self-quenching under operating conditions of DSSC might be smaller than those observed in transient absorption experiments.

4. Conclusions

Complete DSSC made of popular indoline dye D149, TiO_2 or ZnO substrates and commercial iodide-based liquid electrolyte were investigated by time-resolved laser spectroscopy techniques as well as steady-state absorption, scanning electron microscopy, current–voltage and electrochemical impedance measurements. Combining better sensitivity of transient absorption setup and an extended spectral range towards NIR we were able to reveal significant details about the ultrafast dynamics not reported before. We have identified locally excited and charge transfer states of the dye participating in electron injection process, and found a

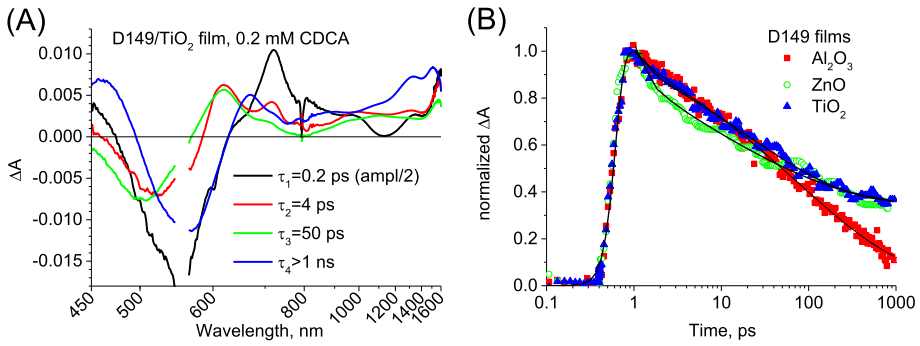

Fig. 6. (A) The wavelength-dependent amplitudes of the components with time constants given in the inset obtained by multi-exponential global fit for D149/TiO_2 with 0.2 mM of CDCA. (B) Kinetic traces of transient absorption measured at 1300 nm for D149 (with 2 mM of CDCA) films on the indicated concentration metal oxides. The pump pulse was 0.5 μJ at 555 nm. The black line shows best fit with parameters given in Table 4C. The time zero is shifted to 1 ps in order to present the time axis in logarithmic scale.

dependence on the observed dynamics on the coadsorbent concentration and excitation energy density. We proposed the explanation for the lower performance with sample aging by electrolyte-induced dye rearrangement and aggregate formation.

We would like to point out that it is commonly assumed that faster decay of the excited state of the dye attached to metal oxide particles in DSSC means faster electron injection and thus better quantum yield of the injection process. However, the situation can be more complex and even opposite. Our studies show that faster decays observed for ZnO cell in comparison to TiO_2 cells are due to enhanced self-quenching of the dyes and in fact the electron injection efficiency is lower in the former than in the latter.

Acknowledgements

This work was supported by NCN (National Science Centre, Poland) under project 2012/05/B/ST3/03284. J. S. is a holder of a scholarship funded within Human Capital Operational Programme, European Social Fund. Dr Maciej Zalas (Faculty of Chemistry, Adam Mickiewicz University in Poznan) is kindly acknowledged for the help in preparation of metal oxide pastes and making the control measurements with solar simulator. We also thank Joanna Bludzinska (Evonik Degussa International AG) for providing us the VP ZnO 20 and P25 nanoparticles. TCSPC studies were made at the Center for Ultrafast Laser Spectroscopy at the A. Mickiewicz University in Poznan, Poland. JAA thanks Abengoa Research for support under collaboration agreement and Junta de Andalucía for funding under grant FQM1851.

Appendix A. Supplementary data

Supplementary data related to this article can be found at http://dx.doi.org/10.1016/j.dyepig.2014.10.008.

References

[1] Horiuchi T, Miura H, Sumioka K, Uchida S. High efficiency of dye-sensitized solar cells based on metal-free indoline dyes. J Am Chem Soc 2004;126:12218–9.
[2] O'Regan B, Grätzel M. A low-cost, high-efficiency solar cell based on dye-sensitized colloidal TiO2 films. Nature 1991;353:737–40.
[3] Hagfeldt A, Boschloo G, Sun L, Kloo L, Pettersson H. Dye-sensitized solar cells. Chem Rev 2010;110:6595–663.
[4] Ito S, Zakeeruddin SM, Humphry-Baker R, Liska P, Charvet R, Comte P, et al. High-efficiency organic-dye-sensitized solar cells controlled by nanocrystalline-TiO_2 electrode thickness. Adv Mater 2006;18:1202–5.
[5] Joly D, Pelleja L, Narbey S, Oswald F, Chiron J, Clifford JN, et al. A robust organic dye for dye sensitized solar cells based on Iodine/Iodide electrolytes combining high efficiency and outstanding stability. Sci Rep 2014;4:4033.
[6] Yang J, Ganesan P, Teuscher J, Moehl T, Kim YJ, Yi C, et al. Influence of the donor size in D–pi–A organic dyes for dye-sensitized solar cells. J Am Chem Soc 2014;136:5722–30.
[7] Yu Q, Wang Y, Yi Z, Zu N, Zhang J, Zhang M, et al. High-efficiency dye-sensitized solar cells: the influence of lithium ions on exciton dissociation, charge recombination, and surface states. ACS Nano 2010;4(10):6032–8.
[8] Mathew S, Yella A, Gao P, Humphry-Baker R, Curchod BFE, Ashari-Astani N, et al. Dye-sensitized solar cells with 13% efficiency achieved through the molecular engineering of porphyrin sensitizers. Nat Chem 2014;6:242–7.
[9] Howie WH, Claeyssens F, Miura H, Peter LM. Characterization of solid-state dye-sensitized solar cells utilizing high absorption coefficient metal-free organic dyes. J Am Chem Soc 2008;130:1367–75.
[10] Snaith HJ, Petrozza A, Ito S, Miura H, Grätzel M. Charge generation and photovoltaic operation of solid-state dye-sensitized solar cells incorporating a high extinction coefficient indolene-based sensitizer. Adv Func Mater 2009;19:1810–8.
[11] Guillén E, Eneko Azaceta E, Peter LM, Zukal A, Tena-Zaera R, Anta JA. ZnO solar cells with an indoline sensitizer: a comparison between nanoparticulate films and electrodeposited nanowire arrays. Energy Environ Sci 2011;4:3400–7.
[12] Fakis M, Stathatos E, Tsigaridas G, Giannetas V, Persephonis P. Femtosecond decay and electron Transfer dynamics of the organic sensitizer D149 and photovoltaic performance in quasi-solid-state dye-sensitized solar cells. J Phys Chem C 2011;115:13429–37.
[13] Guillén E, Peter L, Anta JA. Electron transport and recombination in ZnO-based dye-sensitized solar cells. J Phys Chem C 2011;115:22622–32.
[14] Cappel UB, Feldt SM, Schöneboom J, Hagfeldt A, Boschloo G. The influence of local electric Fields on photoinduced absorption in dye-sensitized solar cells. J Am Chem Soc 2010;132:9096–101.
[15] Fattori A, Peter LM, Wang H, Miura H, Marken F. Fast hole surface conduction observed for indoline sensitizer dyes immobilized at fluorine-doped tin oxide-TiO_2 surfaces. J Phys Chem C 2010;114:11822–8.
[16] Pastore M, De Angelis F. Computational modeling of stark effects in organic dye-sensitized TiO2 heterointerfaces. J Phys Chem Lett 2011;2:1261–7.
[17] Oum K, Lohse PW, Flender O, Klein JR, Scholz M, Lenzer T, et al. Ultrafast dynamics of the indoline dye D149 on electrodeposited ZnO and sintered ZrO2 and TiO2 thin films. Phys Chem Chem Phys 2012;14:15429–37.
[18] Burdziński G, Karolczak J, Ziółek M. Dynamics of local stark effect observed for a complete D149 dye-sensitized solar cell. Phys Chem Chem Phys 2013;15:3889–96.
[19] Wu Y, Marszalek M, Zakeeruddin SM, Zhang Q, Tian H, Grätzel M, et al. High-conversion-efficiency organic dye-sensitized solar cells: molecular engineering on D–A–pi-A featured organic indoline dyes. Energy Environ Sci 2012;5:8261–72.
[20] Anderson NA, Lian T. Ultrafast electron transfer at the molecule-semiconductor nanoparticle interface. Ann Rev Phys Chem 2005;56:491–519.
[21] Wenger B, Grätzel M, Moser JE. Rationale for kinetic heterogeneity of ultrafast light-induced electron Transfer from Ru(II) complex sensitizers to nanocrystalline TiO2. J Am Chem Soc 2005;127:12150–1.
[22] Katoh R, Furube F, Barzykin AV, Arakawa H, Tachiya M. Kinetics and mechanism of electron injection and charge recombination in dye-sensitized nanocrystalline semiconductors. Coord Chem Rev 2004;248:1195–213.
[23] Tachibana Y, Haque SA, Mercer IP, Moser JE, Klug DR, Durrant JR. Modulation of the rate of electron injection in dye-sensitized nanocrystalline TiO2 films by externally applied bias. J Phys Chem B 2001;105:7424–31.
[24] Asbury J, Hao E, Wang Y, Ghosh HN, Lian T. Ultrafast electron Transfer dynamics from molecular adsorbates to semiconductor nanocrystalline thin films. J Phys Chem B 2001;105:4545–57.
[25] Katoh R, Furube A. Electron injection efficiency in dye-sensitized solar cells. J Photochem Photobiol C Photochem Rev 2014;20:1–16.
[26] Benkö G, Kallioinen J, Korppi-Tommola JEI, Yartsev AP, Sundström V. Photoinduced ultrafast dye-to-semiconductor electron injection from nonthermalized and thermalized donor states. J Am Chem Soc 2002;124:489–93.
[27] Ramakrishna G, Singh AK, Ghosh HN, Palit DK. Dynamics of interfacial electron transfer from photoexcited quinizarin (Qz) into the conduction band of TiO2 and surface states of ZrO2 nanoparticles. J Phys Chem B 2004;108:4775–83.
[28] Ye S, Kathiravan A, Hayashi H, Tong Y, Infahsaeng Y, Chabera P, et al. Role of adsorption structures of Zn-porphyrin on TiO2 in dye-sensitized solar cells studied by sum frequency generation vibrational spectroscopy and ultrafast spectroscopy. J Phys Chem C 2013;117:6066–80.
[29] Moser JE. Dynamics of interfacial and surface electron transfer processes. In: Kalyanasundaram K, editor. Dye-sensitized solar cells. 2010 ed. Lausanne: EPFL Press; 2010. p. 403–56.
[30] Thorsmølle VK, Wenger B, Teuscher J, Bauer C, Moser JE. Dynamics of photoinduced interfacial electron transfer and charge transport in dye-sensitized mesoscopic semiconductors. Chimia 2007;61:631–4.
[31] Koops SE, O'Regan BC, Barnes PRF, Durrant JR. Parameters influencing the efficiency of electron injection in dye-sensitized solar cells. J Am Chem Soc 2009;131:4808–18.
[32] Ziółek M, Martín C, Cohen B, Garcia H, Douhal A. Virtues and vices of an organic dye and Ti-doped MCM-41 based dye-sensitized solar cells. J Phys Chem C 2011;115:23642–50.
[33] Giannouli M, Fakis M. Interfacial electron transfer dynamics and photovoltaic performance of TiO2 and ZnO solar cells sensitized with Coumarin 343. J Photochem Photobiol A: Chem 2011;226(1):42–50.
[34] Juozapavicius M, Kaucikas M, van Thor JJ, O'Regan BC. Observation of multi-exponential Pico- to subnanosecond electron injection in optimized dye-sensitized solar cells with visible-pump mid-infrared-probe transient absorption spectroscopy. J Phys Chem C 2013;117:116–23.
[35] Juozapavicius M, Kaucikas M, Dimitrov SD, Barnes PRF, van Thor JJ, O'Regan BC. Evidence for "Slow" electron injection in commercially relevant dye-sensitized solar cells by vis–NIR and IR Pump–Probe spectroscopy. J Phys Chem C 2013;117:25317–24.
[36] Sobuś J, Burdziński G, Karolczak J, Idígoras J, Anta JA, Ziołek M. Comparison of TiO2 and ZnO solar cells sensitized with an indoline dye: time-resolved laser spectroscopy studies of partial charge separation processes. Langmuir 2014;30:2505–12.
[37] Lohse PW, Kuhnt J, Druzhinin SI, Scholz M, Ekimova M, Oekermann T, et al. Ultrafast photoinduced relaxation dynamics of the indoline dye D149 in organic solvents. Phys Chem Chem Phys 2011;13:19632–40.
[38] Fakis M, Hrobárik P, Stathatos E, Giannetas V, Persephonis P. A time resolved fluorescence and quantum chemical study of the solar cell sensitizer D149. Dyes Pigments 2013;96:304–12.
[39] El-Zohry A, Orthaber A, Zietz B. Isomerization and aggregation of the solar cell dye D149. J Phys Chem C 2012;116:26144–53.
[40] El-Zohry A, Zietz B. Concentration and solvent effects on the excited state dynamics of the solar cell dye D149: the special role of protons. J Phys Chem C 2013;117:6544–53.

[41] Wróżowa T, Ciesielska B, Komar D, Karolczak J, Maciejewski A, Kubicki J. Measurements of picosecond lifetimes by time correlated single photon counting method: the effect of the refraction index of the solvent on the instrument response function. Rev Sci Instrum 2004;75(10):3107–21.
[42] Guillén E, Idígoras J, Berger T, Anta JA, Fernández-Lorenzo C, Alcántara R, et al. ZnO-based dye solar cell with pure ionic-liquid electrolyte and organic sensitizer: the relevance of the dye–oxide interaction in an ionic-liquid medium. Phys Chem Chem Phys 2011;13:207–13.
[43] Sakuragi Y, Wang XF, Miura H, Matsui M, Yoshida T. Aggregation of indoline dyes as sensitizers for ZnO solar cells. J Photochem Photobiol A Chem 2010;216:1–7.
[44] Zioł ek M, Karolczak J, Zalas M, Hao Y, Tian H, Douhal A. Aggregation and electrolyte composition effects on the efficiency of dye-sensitized solar cells. A case of a near-infrared absorbing dye for Tandem cells. J Phys Chem C 2014;118:194–205.
[45] Furube A, Katoh R, Yoshihara T, Hara K, Murata S, Arakawa H, et al. Ultrafast direct and indirect electron-injection processes in a photoexcited dye-sensitized nanocrystalline zinc oxide film: the importance of exciplex intermediates at the surface. J Phys Chem B 2004;108:12583–92.
[46] Oum K, Flender O, Lohse PW, Scholz M, Hagfeldt A, Boschloo G, et al. Electron and hole transfer dynamics of a triarylamine-based dye with peripheral hole acceptors on TiO2 in the absence and presence of solvent. Phys Chem Chem Phys 2014;16:8019–29.
[47] de Miguel G, Zió ek M, Zitnan M, Organero JA, Pandey SS, Hayase S, et al. Photophysics of H- and j-aggregates of indole-based squaraines in solid state. J Phys Chem C 2012;116:9379–89.
[48] de Miguel G, Marchena M, Zió ek M, Pandey SS, Hayase S, Douhal A. Femto- to millisecond photophysical characterization of indole-based squaraines adsorbed on TiO2 nanoparticle thin films. J Phys Chem C 2012;116:12137–48.
[49] de Miguel G, Marchena M, Cohen B, Pandey SS, Hayase S, Douhal A. Relating the photodynamics of squaraine-Based DSSCs to the molecular structure of the sensitizers and to the presence of Additives. J Phys Chem C 2012;116:22157–68.
[50] Zió ek M, Burdziński G, Douhal A. Long-living structures of photochromic salicylaldehyde azine: polarity and viscosity effects from nanoseconds to hours. Photochem Photobiol Sci 2012;11:1389–400.